Fuel 261 (2020) 116432

Contents lists available at ScienceDirect

Fuel

journal homepage: www.elsevier.com/locate/fuel

Full Length Article

Influences of natural gas energy fraction on combustion and emission characteristics of a diesel pilot ignition natural gas engine based on a reduced chemical kinetic model

Jun Shu[a], Jianqin Fu[a,b,*], Yongxiang Zhang[a], Mingke Xie[a], Jingping Liu[a], Jianlong Liu[a], Dongjian Zeng[b]

[a] State Key Laboratory of Advanced Design and Manufacturing for Vehicle Body, Hunan University, Changsha 410082, China
[b] Vehicle Measurement, Control and Safety Key Laboratory of Sichuan Province, Xihua University, Chengdu 610039, China

GRAPHICAL ABSTRACT

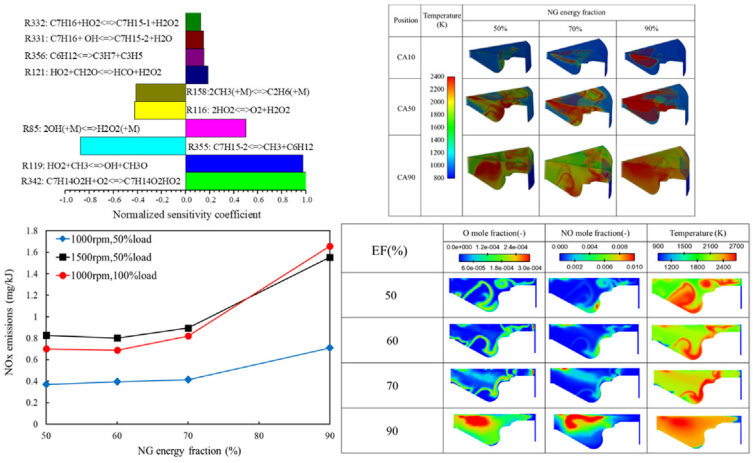

ARTICLE INFO

Keywords:
NG engine
CFD
NG energy fraction
Combustion
Emission
Chemical kinetic

ABSTRACT

In this research, a reduced chemical kinetic mechanism was coupled in computational fluid dynamics (CFD) model to study the detailed influence mechanism of natural gas (NG) energy fraction on the diesel pilot ignition (DPI) NG engines. Based on the CFD model calibrated by experimental data, the impacts of NG energy fraction on the combustion and emission generation processes in DPI NG engine were investigated. The results show that, the start of combustion (SOC) in DPI NG engine is advanced as the NG energy fraction declines and the maximum advance comes up to 4.1°CA at 1000 rpm and 100% load. The deep analysis reveals that the positive influence of R342 on the temperature is the main reason for the shorter ignition delay. The 10–90% combustion duration increases first as the NG energy fraction changes from 50% to 60%, and then decreases if the NG energy fraction further increases. Furthermore, the combustion mode is changed from premixed combustion to non-premixed

Abbreviations: CFD, computational fluid dynamics; CNG, compressed natural gas; DPI, diesel pilot ignition; ECU, electronic control unit; EVO, exhaust valve opening; HRR, heat release rate; ICE, internal combustion engine; ISFC, indicated specific fuel consumption; IVC, intake valve closing; NG, natural gas; SOC, start of combustion; SI, spark ignition

* Corresponding author at: State Key Laboratory of Advanced Design and Manufacturing for Vehicle Body, Hunan University, Changsha 410082, China.
E-mail address: fujianqin@hnu.edu.cn (J. Fu).

https://doi.org/10.1016/j.fuel.2019.116432
Received 10 June 2019; Received in revised form 2 September 2019; Accepted 14 October 2019
Available online 19 October 2019
0016-2361/

combustion with the NG energy fraction decreasing. For the emissions, the NOx emission drops with the decline of NG energy fraction, and the maximum decrease of NOx emission comes up to 0.96 mg/kJ at 1000 rpm and 100% load. The CO emission increases first and then decreases as the NG energy fraction rises from 50% to 90%.

1. Introduction

With the rapid growth of the vehicle stock, the consumption of oil and the massive emissions have become the severe challenges for the energy and environment [1]. Searching alternative fuels to relieve the energy crisis and reduce the engine emissions would be a fast and convenient way [2]. Due to the advantages of low carbon and clean combustion, NG is one of the most feasible alternative fuels to achieve the energy saving and emission reduction [3]. Compared with traditional diesel vehicles, the substitution with NG could reduce the oil use and air pollutant [4,5]. Usually, there are two major pathways to use NG in internal combustion engine (ICE), which are spark ignited NG engine and DPI NG engine [6]. As a popular and economical method, diesel pilot ignited NG could be directly applied in diesel engine with simply modification of intake apparatus [7]. Simultaneously, the greater the proportion of NG in the fuel (NG-diesel dual fuel), the more oil will be saved and less soot emissions will be produced [8]. Consequently, the NG has been extensively applied in vehicle transport system.

The combustion mode of DPI NG in ICE has a promising future and it has received many attentions from both scholars and engineers [9]. Meng et al. [10] explored the possibility of reducing emissions in diesel/CNG (compressed natural gas) dual-fuel engine through the diesel and n-butanol blends as the pilot fuel. The experimental data revealed that B20CNG70 (at 70% CNG substitution rate) can significantly reduce the NOx emission and the addition of n-butanol results in the trade-off between CO and THC emissions. Zheng et al. [11] experimentally studied the impact of equivalence ratio on a low compression ratio of 14.2 in DPI NG engine. The results showed that the rise of heat release rate (HRR) and exhaust gas temperature while the decline of combustion duration were obtained because of the increase of equivalence ratio in DPI NG mode. Chen et al. [12] experimentally evaluated the performance and emissions of a methanol/NG dual fuel spark-ignition engine. As the methanol energy substitution ratio increases, the maximum HRR, peak in-cylinder pressure and temperature become larger. In addition, the brake thermal efficiency increases but the equivalent brake specific fuel consumption decreases significantly with methanol enrichment. Yang et al. [13] carried out an experiment to research the behavior of the particles in a DPI NG engine with varying loads at constant speed. The results indicated that the particle size distribution is not sensitive to the variation of pilot injection pressure and the particle number concentration could be reduced dramatically with increased pilot injection pressure as well as engine loads. Castro et al. [14] implemented an experiment to study the emissions and maximum substitution of diesel by hydrogen in a diesel engine. According to the results, brake fuel conversion efficiency declines with the rise of hydrogen at all the engine loads and the NO emission decreases with the rise of hydrogen at low engine load. Abagnale et al. [15] discussed the impact of the fuel ratios variation on the combustion and pollutant in a dual fuel engine. The results revealed that the lowest pollutant and CO_2 appear at nearly 50% of CH_4 ratio and as the CH_4 ratios are higher than 75%, the conditions are close to knocking and the NOx has a relevant increase.

With the rapid development of chemical reaction mechanism and computational resource, researchers began to pay more attention to the deep analysis of mechanism, instead of simply staying on the analysis of the experimental phenomenon [16]. Through the 3-D CFD coupling with NG and diesel combustion mechanism, it is very convenient to obtain the behavior of those reactions and search the most important reaction if some parameters are changed. Liu et al. [17] optimized the injection parameters of direct injection NG engine through CFD code with genetic algorithm, and claimed that the developed gas fuel injection model is able to predicate the penetrations of the NG injection. Besides, the lowest indicated specific fuel consumption (ISFC) condition can be achieved when the injection interval between the diesel and NG is 1.38 °CA, and the later of the gas injection timings leads to the higher soot emissions cases. Jung et al. [18] considered an absorbing way to reduce the emissions in a dual fuel engine, and found that the brake power decreases and NOx emissions decline with increase of the NG energy proportion. Cameretti et al. [19] calculated the combustion and emission process of dual fuel engine at different injection timings, and stated that advancing the diesel injection timing results in better combustion efficiency and the increase of NOx with a sharper in-cylinder pressure rise. Zhou et al. [20] investigated the soot evolution at different CNG substitution ratios through KIVA-3V R2 with a new soot model. The results displayed that the soot emissions get drastically reduced with the rise of CNG substitution ratio and the soot mass of CNG70 is less than the other two cases because of the decrease of pyrene distribution, which leads to a reduced generation of soot precursors.

Many researches have been conducted on dual fuel engines while the research about DPI NG engines fails to go deep insight about the reasons for the phenomenon. According to Refs. [21,22], the injection angle and timing of NG-diesel fuel engine have significant effects on combustion and emission characteristics, but few comprehensive researches have been dedicated to computationally investigate the effects of NG energy fraction on DPI NG engine. Although numerous literatures have been reviewed, the study which uses the kinetic mechanism to analyze the combustion and emissions of DPI NG engines with a large range of NG energy fraction is rare. Especially, the important reactions on the combustion process and emission formation of DPI NG engines with the variation of NG energy fraction could not be found. Hence, it is necessary to carry out an investigation about the influences of NG energy fraction on the behavior of in-cylinder mixture by the 3-D CFD software CONVERGE embedding in chemical kinetic mechanisms, which can display the variation process and 3-D distribution of fuel consuming and emissions producing. This study aims to explain the fuel combustion process and emissions generation with the variation of NG energy fraction and take it as a basis to optimize the combustion and emission performance of DPI NG engines.

2. Experiment and simulation model

2.1. Testing process

For the sake of studying the NG-diesel dual fuel mode, a six-cylinder common rail system diesel engine has been modified into the DPI NG engine. The electronic control unit (ECU) of the diesel engine has been handled and the NG was supplied in the intake system. A list of the engine's main parameters is presented in Table 1 and the compositions of natural gas is displayed in Table 2. To distinctly clarify the experiment process, the engine test bench and experimental scenario are displayed in Fig. 1. The detailed test instruments and their precision could be seen in Ref. [21]. When the engine was modified, the gas mixer was installed before the throttle valve so as to blend the NG and air. Three engine operational conditions, which are 50% load and 100% load at 1000 rpm and 50% load at 1500 rpm, were chosen to implement the experiment as they were representative conditions in ICE. After the temperature of engine coolant reached to 70 ℃, the three typical conditions were measured. In order to calibrate the CFD model, a lot of

Table 1
Basic parameters of the experimental engine.

Item	Content
Bore (mm)	126
Stroke (mm)	130
Connecting rod length (mm)	219
Original compression ratio	17.0
Displacement (L)	9.726
Rated power (kW)/Speed (rpm)	247/1900
Maximum torque (N·m)/Speed (rpm)	1550/(1200–1500)
Injector nozzle spray angle (°)	147
Number of injector holes	8

Table 2
The compositions of natural gas.

Compositions	Proportion (%)
Methane	98.5
Ethane	0.56
Propane	0.09
n-Butane	0.029
Isobutane	0.017
Pentane	0.006
Hydrogen sulfide	0.005
Carbon dioxide	0.51
Nitrogen	0.283

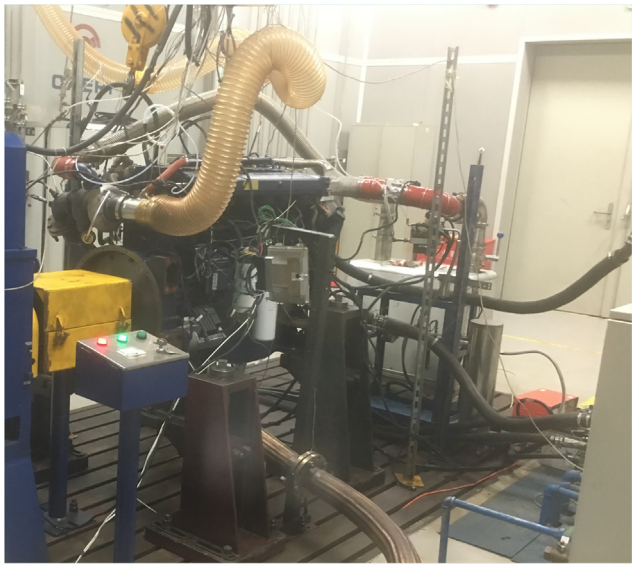

Fig. 1. The engine test bench and experimental scenario of DPI NG engine.

Table 3
Uncertainties of measured and calculated parameters.

Parameters	Uncertainty (%)
Pressure	0.5
Engine speed	0.5
Indicated thermal efficiency	1.1
HC and NOx emissions	1.0

engine parameters were obtained, including NG flow rate, in-cylinder pressure, intake temperature and pressure, emissions of NOx, CO, HC, etc.

Additionally, an uncertainties analysis for the experimental results, like in-cylinder pressure and indicated thermal efficiency, was conducted based on the root mean square method [23]. The uncertainty in measured variables was determined by using Formula (1).

Table 4
Physical models in the simulation.

Physical Parameters	Model
Turbulence modeling approach	Reynolds Averaged Navier-Stokes (RANS) [26,27]
Turbulence model	Han and Reitz [28]
NG and diesel chemistry	Methane and n-heptane (76 species and 464 reactions) [24]
Combuation	SAGE model [29]
Drop evaporation	Frossling model [30]
Drop coalescence	Post collision outcomes model [31]
Drop collision	NTC method [32]
Spray break-up	Kelvin-Helmholtz and Rayleigh-Taylor (KH-RT) model [33]
Drop/wall interaction	Rebound/slide model [34]
NOx emissions	Extended Zeldovich mechanism [35]

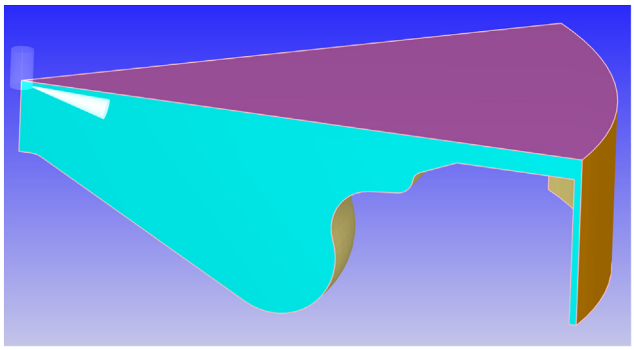

Fig. 2. The geometry of the simulated combustion chamber.

$$U_R = \left[\left(\frac{\partial R}{\partial x_1}U_{x_1}\right)^2 + \left(\frac{\partial R}{\partial x_2}U_{x_2}\right)^2 + \ldots\left(\frac{\partial R}{\partial x_n}U_{x_n}\right)^2\right]^{1/2} \quad (1)$$

where the uncertainty is measured in R, x_n are independent variables with measured uncertainties, and U_{x_1}, U_{x_2}, U_{x_n} are error limits of measured parameters. The details of the uncertainties are given in Table 3.

2.2. Physical sub-models in CFD model

The CONVERGE software was used to calculate the combustion, thermodynamics, chemical reaction and emission production process in a DPI NG engine at different NG energy fraction. In the simulation process, a reduced chemical kinetics mechanism was used to display all elementary reaction of the in-cylinder mixture combustion, and the mechanism validation has been discussed in Ref. [24]. In this chemical mechanism, n-heptane was chosen to represent diesel and methane was chosen to represent NG. Although the light alkanes could shorten the ignition delay in NG [25], it has a very small proportion in the NG (as shown in Table 2) and can be ignored when discuss the influence of NG energy fraction on the DPI NG engine. Meanwhile, the Extended Zeldovich mechanism was chosen to calculate the NOx emission. Additionally, the gas flow and spray process were simulated by a number of sub-models, and these models are presented in Table 4. In addition, the detailed reasons for the choosing of these models could be seen in Ref. [21].

2.3. CFD model validation

For sampling the calculation process, the closed-cycle, which is from the intake valve closing (IVC) to exhaust valve opening (EVO), was chosen to simulate the behavior of in-cylinder mixture of the DPI NG engine. Simultaneously, as the distribution of eight nozzle holes of the injection is symmetrical in the central axis, one-eighth of the combustion chamber model was considered. Hence, as shown in Fig. 2, only

Table 5
The detail data of initial conditions and boundary conditions.

	Load	Speed (rpm)	Initial pressure (bar)	CH_4 mass (mg)	λ	EF (%)	Injection duration (°)	Injection timing (°BTDC)	Piston (K)	Cylinder (K)	Head (K)
Case 1	50%	1000	1.359	69.05	1.511	92.16	3	8	553	433	523
Case 2	50%	1500	1.499	86.36	1.324	93.63	4.5	11			
Case 3	100%	1000	2.006	126.49	1.24	95.56	3	5			

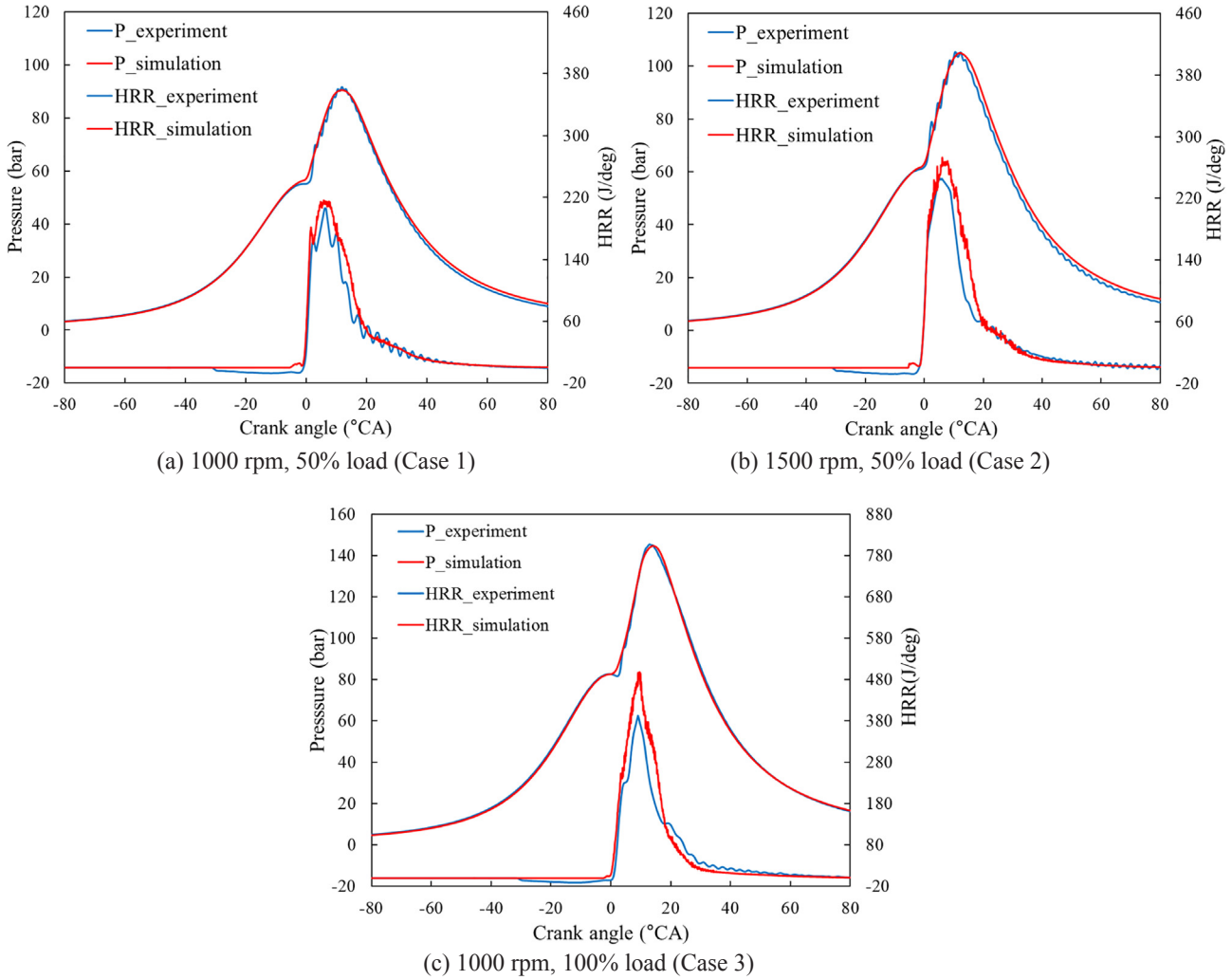

Fig. 3. The contrast of experimental and calculated results (in-cylinder pressure and HRR).

one spray is located in the geometry and the simulation time could be saved largely. During the mesh generation process, the size of the basic grid was set to 1.8 mm and the adaptive mesh refinement method was adopted to obtain sufficient fine grid and eliminate sub-grid effects. For the accuracy simulation, the boundary conditions and initial data of the model are from the experimental results and the detailed parameter settings for different engine conditions are listed in Table 5. In order to improve the combustion and emission characteristics of DPI NG engines with the change of NG energy fraction, a bigger scope of NG energy fractions (which are 50%, 60%, 70% and 90%) were selected to search the behaviors of in-cylinder mixture of the DPI NG engine.

Before the analysis of the impact of the NG energy fraction on the in-cylinder combustion and emission characteristics in a DPI NG engine, the NG energy fraction is defined as follows, which is the ratio of the energy content of the NG to the total energy of fuel (NG and diesel).

$$EF = \frac{m_{NG} \cdot H_{u,NG}}{m_{NG} \cdot H_{u,NG} + m_{diesel} \cdot H_{u,diesel}} \times 100\% \quad (2)$$

where m_{NG} and m_{diesel} are the mass of NG and diesel, respectively; $H_{u,NG}$ and $H_{u,diesel}$ are the low heating value of NG and diesel, respectively.

To verify the validity of the CFD model, simulated results of the DPI NG engine are compared with the corresponding measured data. Fig. 3(a)–(c) show the comparison of simulated and measured combustion characteristic parameters (in-cylinder pressure and HRR). As shown, the calculated in-cylinder pressure matches the experimental results very well in all three cases. Although the calculated HRR is beyond the margin of error at some points (e.g., the peak HRR in Fig. 3(c)), it is still acceptable due to the same variation trends between the calculated and measured HRR in the whole combustion duration. Simultaneously, the comparisons of NOx, HC and CO emissions between experimental data and calculated results are displayed in Fig. 4. For NOx and CO emissions, the relative errors between the experimental and calculated results are small, which means that the CFD model has satisfactory accuracy on the two kinds of emissions. Because the simulated HC is located in the cylinder and the HC still could be oxidized in the exhaust pipe, the simulated HC is obviously larger than

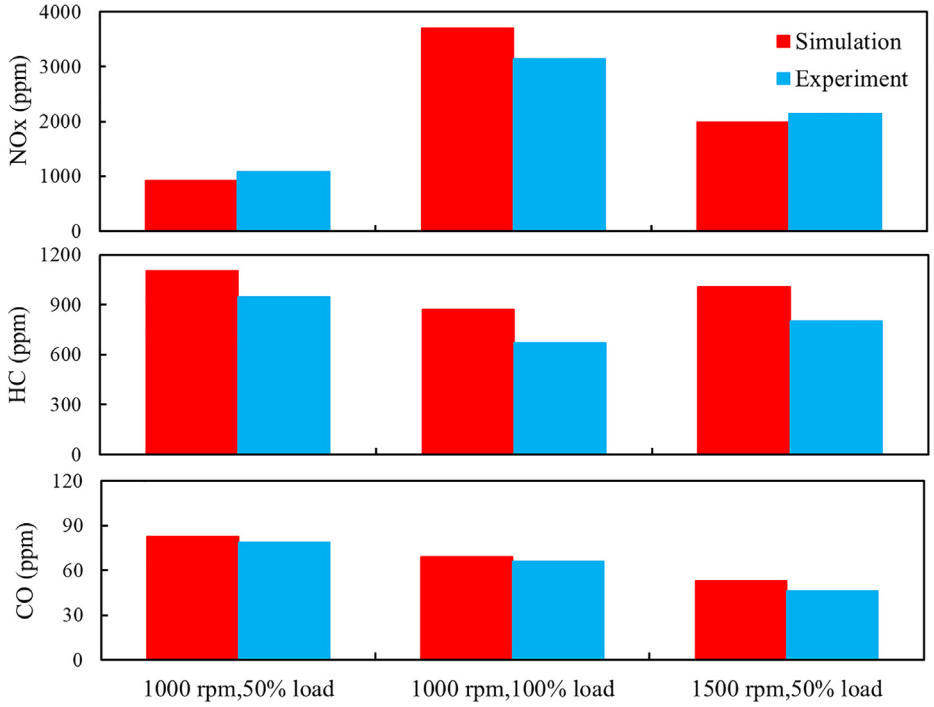

Fig. 4. The contrast of experimental and calculated emissions.

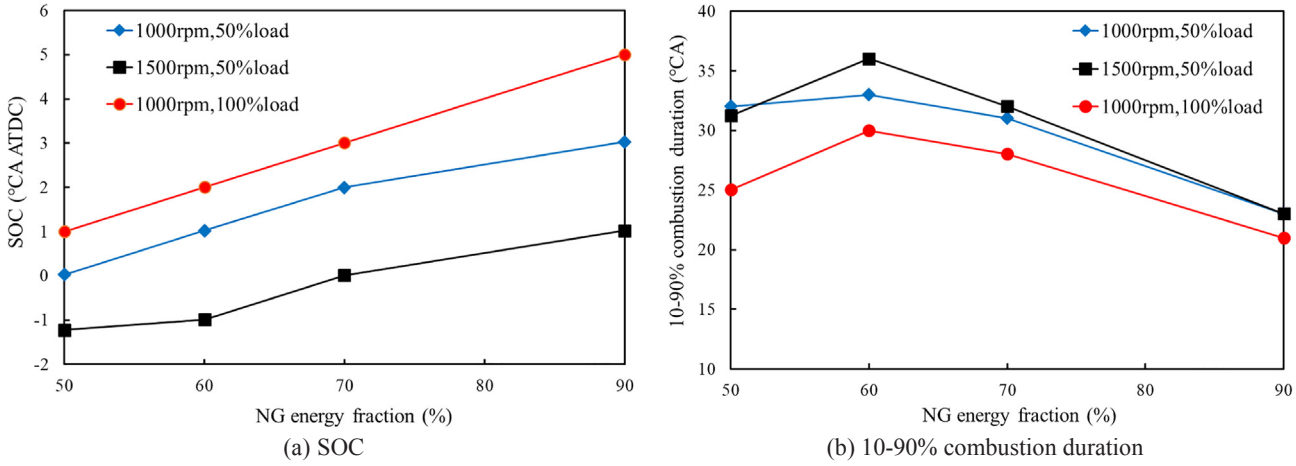

Fig. 5. Combustion parameters versus NG energy fraction in three cases.

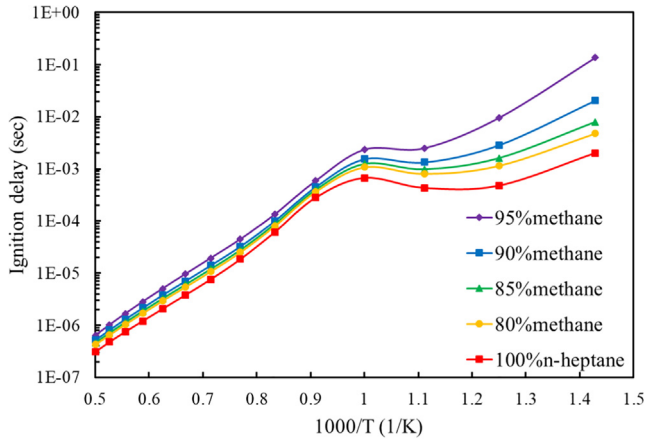

Fig. 6. Ignition delay of methane and n-heptane at different mole fraction.

that tested in the exhaust pipe. Despite larger difference is observed between the experimental and calculated HC emissions, the variation trends in both are similar. Therefore, the calibrated cases are accurate and effective enough, which can be used to study the effects of the NG energy fraction on the in-cylinder combustion and emission characteristics in a DPI NG engine.

3. Results and discussions

3.1. Impact of NG energy fraction on the combustion characteristic

To describe the impact of NG energy fraction on the in-cylinder combustion process, the main combustion parameters in the DPI NG engine, like SOC and 10–90% combustion duration, are discussed. Additionally, the position with 10% of the total heat released is defined as the SOC. Fig. 5(a) and (b) display the SOC and 10–90% combustion duration at various NG energy fraction. As shown in Fig. 5(a), the SOC of the DPI NG engine is advanced as the NG energy fraction decreases

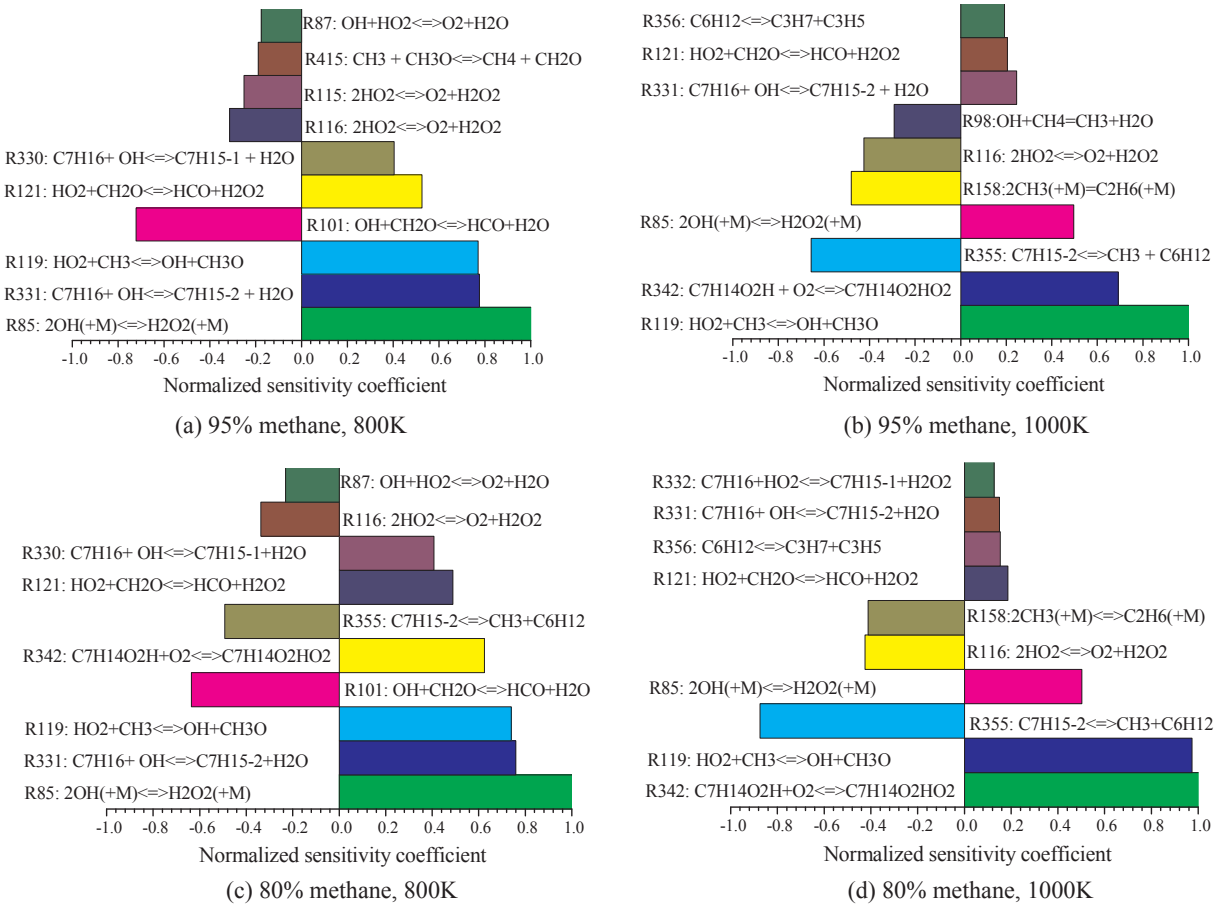

Fig. 7. Temperature A-factor sensitivities at the time of ignition for methane and n-heptane mixtures.

and the maximum advance of SOC reaches up to 4.1 °CA in Case 3. According to the relative researches [36–39], the kinetic modeling could effectively display the ignition delay in dual fuel. To deeply analyze this phenomenon, the contrast of calculated ignition delay periods in different mole fractions of methane and n-heptane is displayed in Fig. 6. It should be noted that the ignition delay is calculated through the Chemkin-Pro software in a given adiabatic system. The initial condition is homogeneous at 50 bar and the equivalence ratio is equal to 1.0. In the transient calculation process, once the temperature reaches a value 400 K higher than the initial temperature, it is defined as the state of ignition. As shown in Fig. 6, when the initial temperature is higher than 1000 K, the impact of the methane mole fraction on the ignition delay is very little. On the contrary, the difference among various methane mole fractions is obvious. This issue is explained as follows. In low temperature conditions, the temperature fails to overcome the activation energy barrier of NG, but the NG can be ignited by diesel components. And the chain branching reaction of diesel at low temperature depends on the radical species formed directly from the parent fuel [40]. That means more diesel species result in faster chemical reaction rates at low temperature. The same phenomenon can also be found in Ref. [41]. Therefore, in low temperature conditions, the ignition delay shows significant difference as the methane mole fraction changes.

In addition, a temperature sensitivity research was performed with 95% and 80% methane mole fraction at 800 K and 1000 K so as to analyze the impact of methane mole fraction on the chemical reaction [42,43]. As shown in Fig. 7(a) and (c), the effects of the top four sensitive reactions (R85, R331, R119 and R101) on the temperature are same at 800 K. Nevertheless, one more positive impact on the temperature occurs in 80% methane, which is the R342: $C_7H_{14}O_2H + O_2 \Leftrightarrow C_7H_{14}O_2HO_2$. It is noteworthy that the R342 is an important branching reaction, in which the peroxy-alkylhydroperxy radical is produced through the alkyl-hydroperoxy radical and oxygen. This path promotes the formation of ketohydroperoxide species that are the branching agents producing new radicals, such as $C_5H_{11}CHO$ and CH_2O [44]. Meanwhile, the impacts of the top four sensitive reactions (R342, R355, R119 and R85) on the temperature are also same at 1000 K between Fig. 7(b) and (d). Furthermore, the R342 becomes the most sensitive reaction in 80% methane. That is to say, at the same initial temperature, the decrease of methane mole fraction makes the ignition delay shorter which is mainly due to the positive influence of R342 on the temperature. Considering that the in-cylinder compression temperature is between 800 K and 1000 K (as shown in Fig. 8) at the time of fuel injection in the DPI NG engine, the retard of SOC is mainly influenced by the R342 as the NG energy faction increases.

In Fig. 5(b), the 10–90% combustion duration increases first as the NG energy fraction rises from 50% to 60%, and then decreases when the NG energy fraction further increases. This result is different from the previous research [45] as it only studied the effect of lower NG energy fraction. Simultaneously, the maximum gap of 10–90% combustion duration comes up to 10 °CA, 12.6 °CA and 9 °CA in Case 1, Case 2 and Case 3, respectively. Because the higher temperature leads to the faster propagation velocity of turbulent flame [46], the flame propagation velocity in the 90% NG energy fraction reaches the maximum value (the mean in-cylinder temperature of the DPI NG engine is shown in Fig. 8(a)–(c)). Nevertheless, in the condition of 50% NG energy fraction, the fuel which would release 90% total released heat concentrates near the spray as the spray contains 50% energy. This causes the main combustion process to mainly concentrate near the spray and the flame propagation speed to become unimportant. So, the 10–90%

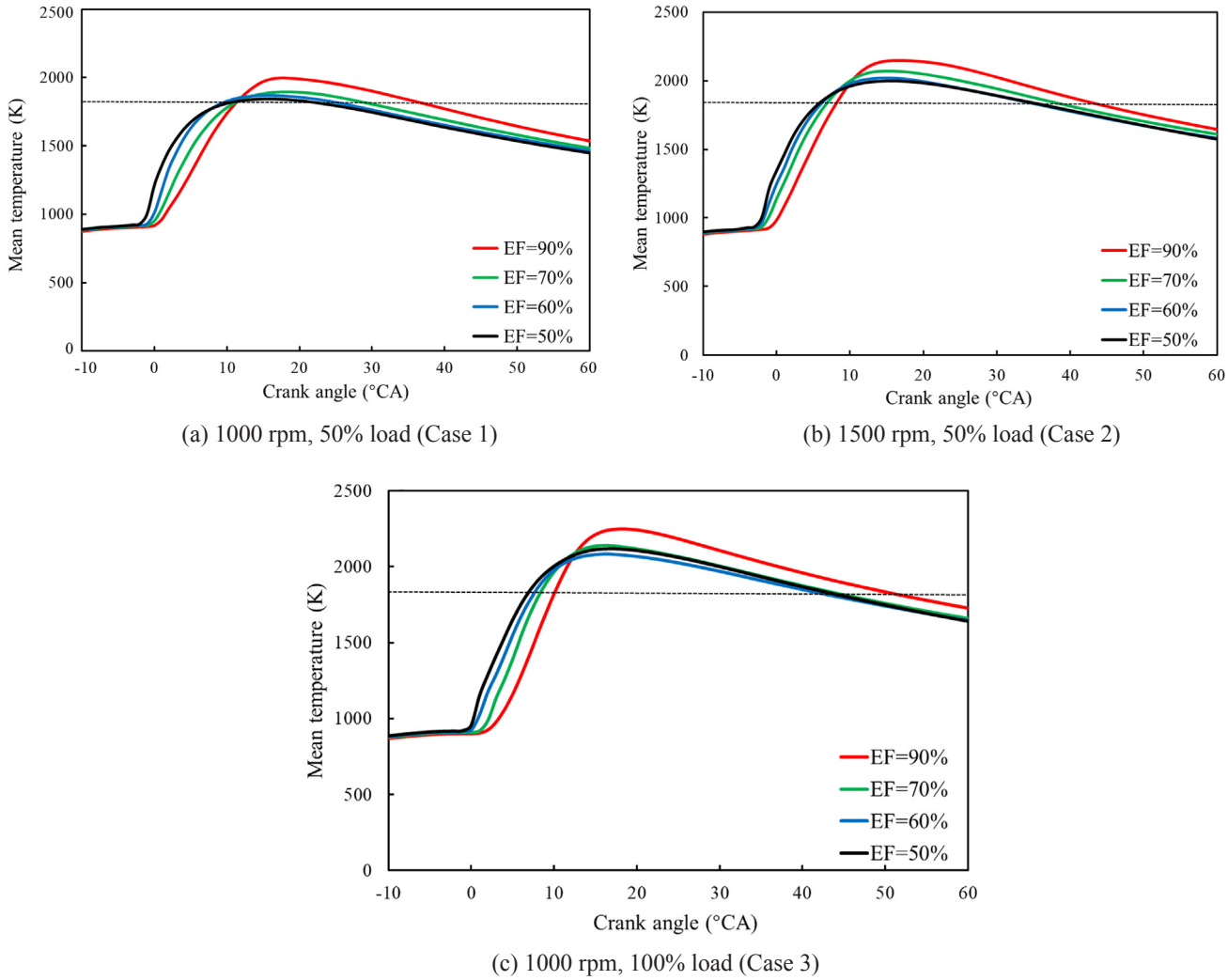

Fig. 8. The average in-cylinder temperature at various NG energy fraction.

combustion duration in 50% NG energy fraction is shorter than that in 60% NG energy fraction. To demonstrate the above analysis, the in-cylinder temperature field of this DPI NG engine is presented in Fig. 9. It is obvious that the high temperature zone gradually spreads to the cylinder wall in 90% NG energy fraction, which makes the combustion process similar to the spark ignition (SI) combustion mode. Meanwhile, in the condition of lower NG energy fraction, the high temperature zone concentrates near the spray in CA10 and CA50, which makes the combustion mode approach to the diesel combustion mode.

3.2. Effect of NG energy fraction on emissions

In this section, the NOx, CH_4 and CO emissions in the DPI NG engine with the variation of NG energy fraction are discussed. In order to better indicate the relationship between the amount of emissions and the energy, the unit of "mg/kJ", which means the mass of emission produced as 1 kJ fuel energy is released, is chosen to discuss the emissions. Fig. 10 presents the NOx emission versus NG energy fraction in three cases. In general, the NOx emission goes up with the increase of the NG energy fraction. Compared with the Case of 50% load, the increasing trend of NOx emission is more obvious at 100% load. In Case 3, the NOx emission is increased by 0.96 mg/kJ as the NG energy fraction rises from 50% to 90%. It can be known from Ref. [35] that NO is the main component in NOx emissions, which takes up more than 90%. Although there are four kinds of NOx formation mechanisms, which are thermal-NO, prompt-NO, NNH and N_2O routes, the thermal-NO is more suitable to predict the NO formation in internal combustion engines. Thus, in this study, the thermal-NO mechanism was considered and used to explain the variation of NOx emission. In the thermal-NO mechanism, the main influence factors are the in-cylinder temperature and oxygen concentration [35]. The variation of NO mole fraction and O mole fraction in Case 3 is presented in Fig. 11, which can be used to deeply analyze the influence factor of NO emission. Firstly, as shown in Fig. 8, the maximum mean in-cylinder temperature becomes higher as the NG energy fraction increases. Secondly, the atomic oxygen mole fraction reaches the highest level at the largest NG energy fraction (see Fig. 11). Because the higher atomic oxygen mole fraction is helpful for the formation of NO in the thermal-NO mechanism, the highest oxygen atoms mole fraction corresponds to the highest NO mole fraction (both of which appear in the 90% NG energy fraction, as shown in Fig. 11). Finally, according to the analysis of Hill and Smoot [47], when the temperature is higher than 1800 K and the excess air coefficient is larger than 1.0, the NO formation reaction is more likely to occur. Due to the above reasons, the NOx emission of the DPI NG engine increases as the NG energy fraction becomes larger.

For further analyzing the influence factor of NOx emissions from the thermal-NO mechanism, the spatial distributions of the temperature, NO and O mole fraction at different NG energy fraction in Case 3 are presented in Fig. 12. Through the comparison between O mole fraction and temperature at 20 °CA ATDC, it can be found that the zone of

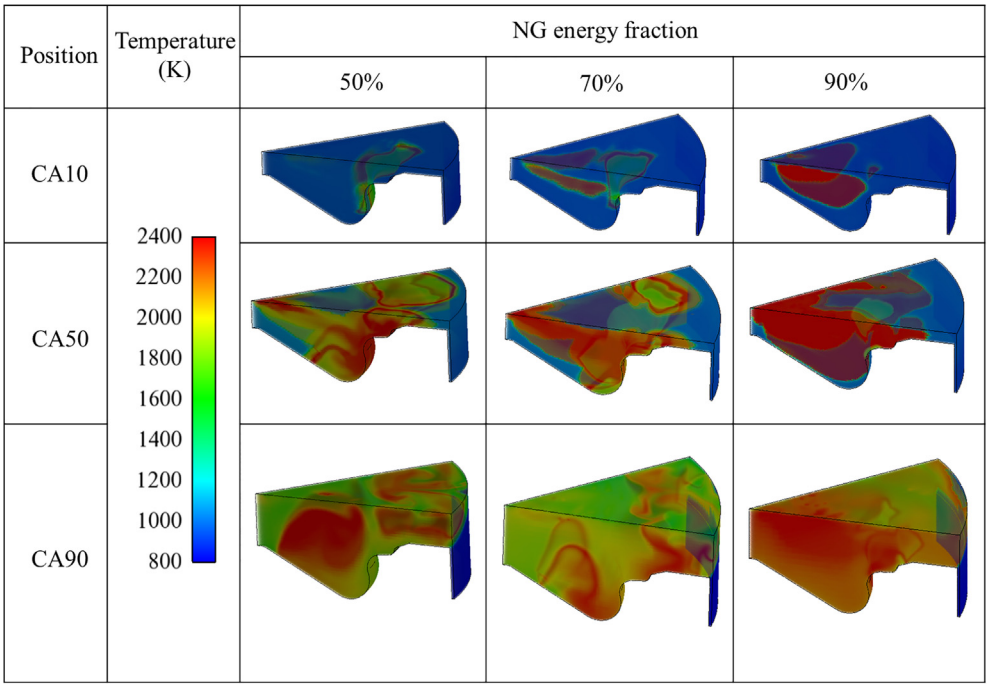

Fig. 9. The in-cylinder temperature distribution at CA10, CA50 and CA90 in Case 3.

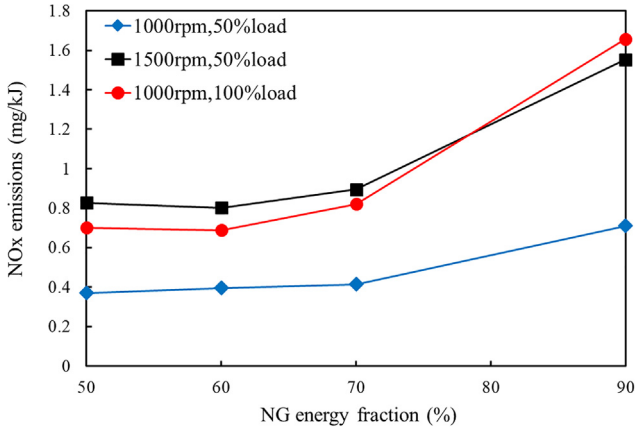

Fig. 10. NOx emissions versus NG energy fraction in three cases.

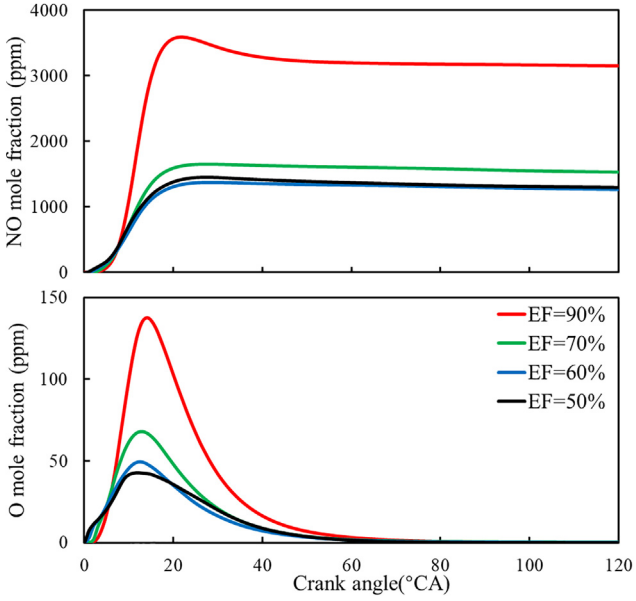

Fig. 11. The variation of in-cylinder O and NO mole fraction in Case 3.

higher oxygen atoms concentration mainly locates in the high temperature zone. Although a part of the oxygen atoms appear near the flame front, they would be consumed during the flame propagation. In both high temperature and flame front zones, the oxygen atoms are formed by the reaction (R1) and consumed by the methane combustion near the flame front, which is helpful to generate more NO through reaction (R2) in the high temperature zone. As shown in Fig. 12, the area of the high temperature zone reaches the maximum value in 90% NG energy fraction. As a result, the NOx emission in 90% NG energy fraction is significantly larger than that in other NG energy fractions.

$$H + O_2 \leftrightarrow O + OH \quad \text{(R1)}$$

$$O + N_2 \leftrightarrow NO + N \quad \text{(R2)}$$

The CO emission in the DPI NG engine in three cases is displayed in Fig. 13. In general, the CO emission first increases and then declines as the NG energy fraction rises from 50% to 90%. In Case 3, the highest CO emission in 60% NG energy fraction is 16 times higher than that in 90% NG energy fraction. According to the chemical reaction mechanism of CO oxidation [48], the CO species are actually consumed by reacting with OH radicals (R4), which is also a chain-propagating reaction. It can be found in the further analysis that OH radicals are mainly produced by the reaction (R5). Thus, there are not enough OH radicals for reacting with CO species when the excess air coefficient is smaller than 1.0. To clearly explain this issue, the CO mole fraction and excess air coefficient at different NG energy fraction in Case 3 are displayed in Fig. 14. As shown, the CO emission appears in the zone of lower lambda at the time of exhaust valve opening (120°CA ATDC). Although a few CO emission appears in the flame propagation (as shown in the 5°CA and 10 °CA ATDC of Fig. 14), it is consumed by the oxygen in the combustion process. Simultaneously, the lowest excess air coefficient occurs in the 70% NG energy fraction at 120°CA ATDC, which is mainly affected by the spray. This leads that the CO emission is remarkably higher than that in 50% and 90% NG energy fraction. This phenomenon is different from that in Ref. [45], in which the CO emission increases

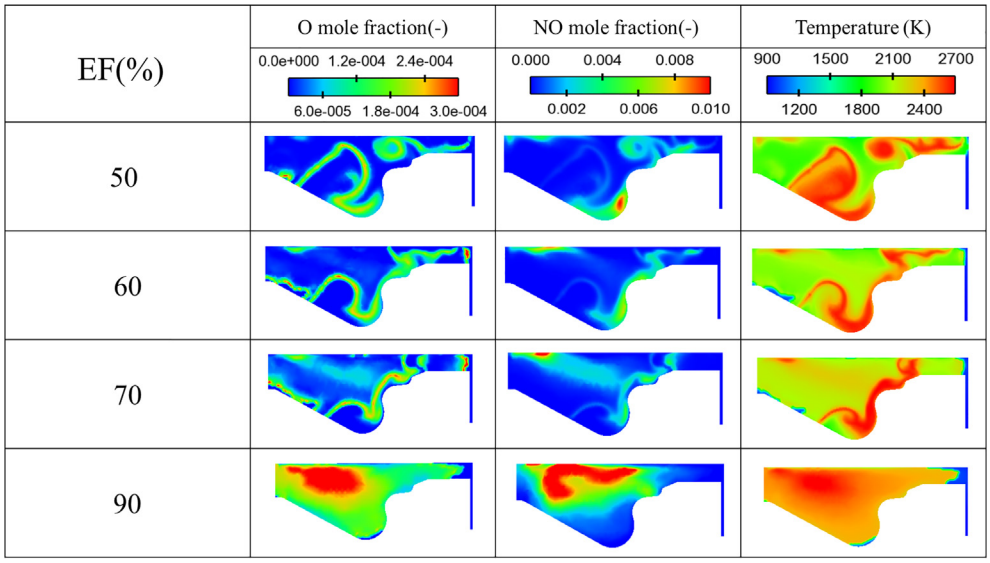

Fig. 12. The distribution of temperature and mole fraction of O and NO at 20 °CA ATDC in Case 3.

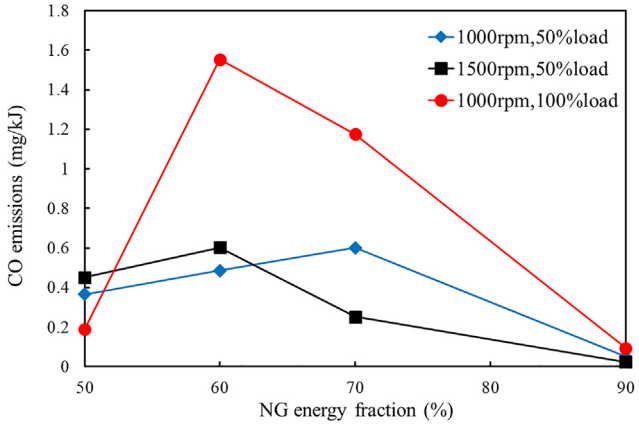

Fig. 13. The CO emission at different NG energy fraction in three cases.

with the rise of the NG energy fraction. As the diesel takes a small part proportion (the energy fraction is less than 30%), more homogeneous mixed gas will be burned, which leads less fuel to appear in the zone of lower excess air coefficient. So, the variation trend of CO emission in higher NG energy fraction has not been found in Ref. [45].

$$CO + O_2 \leftrightarrow CO_2 + O \quad \text{(R3)}$$

$$CO + OH \leftrightarrow CO_2 + H \quad \text{(R4)}$$

$$H + O_2 \leftrightarrow OH + O \quad \text{(R5)}$$

Although there are many species in HC emissions, the CH_4 emission accounts for more than 90% in the DPI NG engine [49]. Thus, the unburned methane could represent the total HC emissions in this study. The influences of NG energy fraction on the unburned methane emission in three conditions are displayed in Fig. 15. In general, the unburned methane increases with the ascent of NG energy fraction and the variation of methane emission is remarkable at 50% load but small at 100% load. The highest difference of methane emission reaches to 0.83 mg/kJ in Case 1 (1000 rpm and 50% load). The main reason is that the increase of methane mole fraction leads more unburned methane to concentrate in the chamber crevice. In addition, due to the difference between the in-cylinder wall and gas temperature, the gas near the cylinder wall is rapidly cooled, which leads to the occurrence of quenching effect and the generation of a large amount of unburned HC emission. Since the quenching effect is more obvious at low speed and low load, the unburned HC emission at 1000 rpm and 50% load is obviously higher than that in the other two conditions. At 100% load, the methane emission reaches the lowest level in all three cases regardless of the variation of NG energy fraction. This is because the higher load corresponds to the higher in-cylinder temperature (see Fig. 8), which can accelerate the oxidation of methane. Meanwhile, when the NG energy fraction is below 70%, the variation of the methane emission becomes very small. The reason is that the increase of diesel energy fraction leads to the decline of the importance of the flame propagation. Therefore, the unburned methane increases with the ascent of NG energy fraction.

4. Conclusions

In this research, the influences of NG energy fraction on the in-cylinder combustion and emission characteristics of a DPI NG engine were analyzed under three typical engine conditions. Through the deep analysis with the chemical reaction mechanism, some helpful conclusions can be acquired as follows.

(1) During the combustion process, the SOC in the DPI NG engine is advanced as the NG energy fraction declines and the maximum advance of SOC comes up to 4.1 °CA at 1000 rpm and 100% load. When the initial temperature is less than 1000 K, the methane mole fraction has an obvious effect on the ignition delay. In addition, the positive influence of R342 on the temperature is the main reason for the reduction of ignition delay. Therefore, the retard of SOC is mainly impacted by the R342 as the NG energy faction increases in the DPI NG engine.
(2) The 10–90% combustion duration increases first as the NG energy fraction changes from 50% to 60%, and then decreases when the NG energy fraction continues to increase. Meanwhile, the maximum gap of 10–90% combustion duration comes up to 10 °CA, 12.6 °CA and 9 °CA in the three cases, respectively. At 90% NG energy fraction, the high temperature zone gradually spreads to the cylinder wall, which makes the combustion process similar to the SI combustion mode. In the condition of lower NG energy fraction, the high temperature zone concentrates near the spray in CA10 and CA50. Thus, the combustion mode changes from premixed combustion to non-premixed combustion with the NG energy fraction decreasing.
(3) For the emissions, the NOx emission of the DPI NG engine becomes more with the rising of NG energy fraction because of the increased

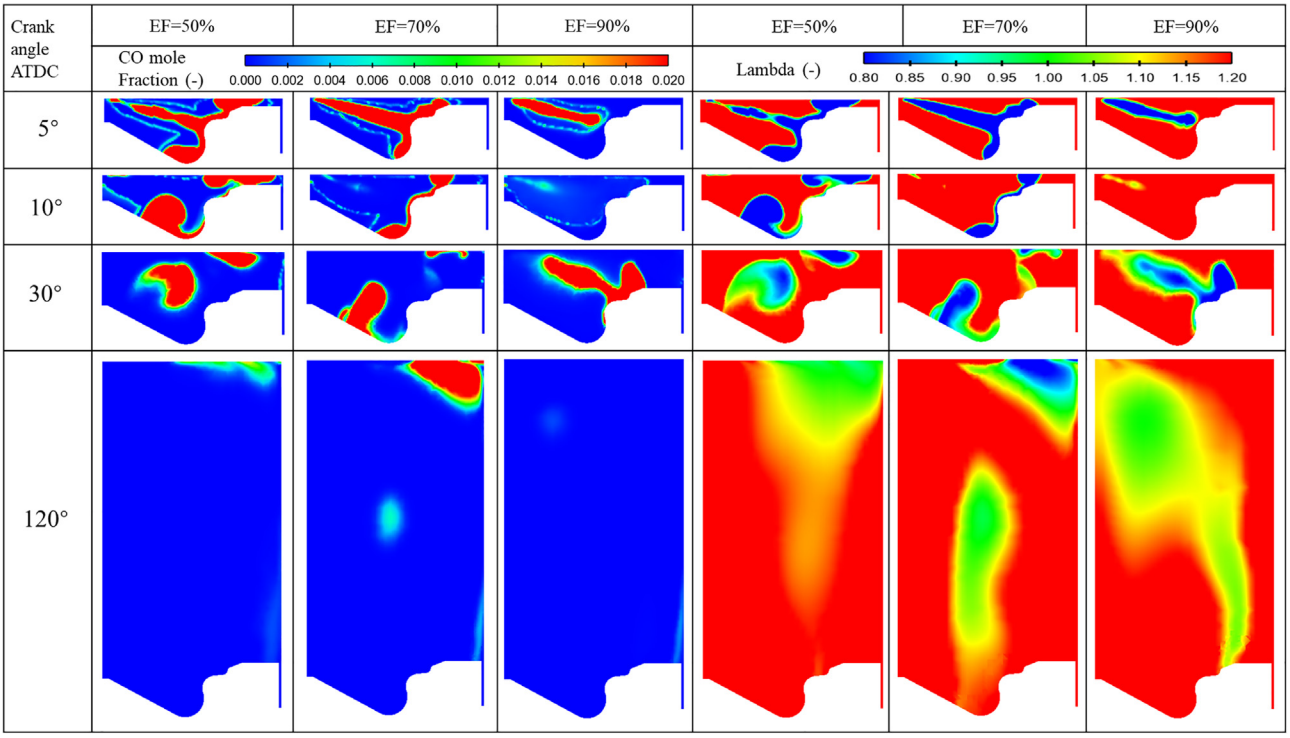

Fig. 14. Lambda and CO mole fraction at different NG energy fraction in Case 3.

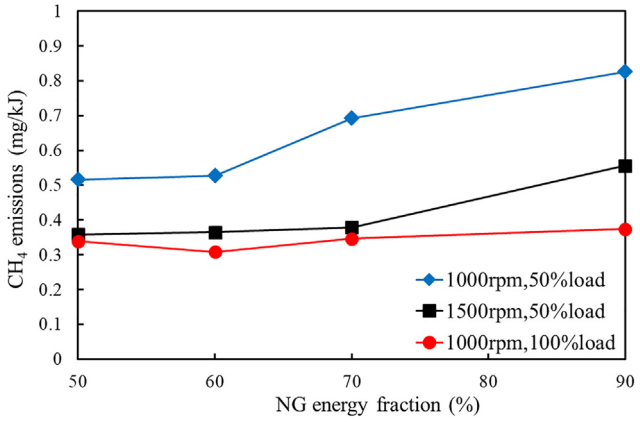

Fig. 15. The CH_4 emission at different NG energy fraction in three cases.

in-cylinder mean temperature and oxygen concentration. At 1000 rpm and 100% load, the NOx emission is increased by 0.96 mg/kJ as the NG energy fraction rises from 50% to 90%. The CO emission first increases and then decreases as the NG energy fraction rises from 50% to 90%. At the same time, the unburned methane increases with the ascent of NG energy fraction and the variation of methane emission is remarkable at 50% load but not obvious at 100% load. At 1000 rpm and 50% load, the highest difference of the methane emission reaches to 0.83 mg/kJ due to the variation of NG energy fraction.

Acknowledgements

This research work is jointly sponsored by the National Natural Science Foundation of China (No. 51876056), the Open Research Fund of Vehicle Measurement, Control and Safety Key Laboratory of Sichuan Province, Xihua University (No. SZJJ2016-079), the Fundamental Research Funds for the Central Universities and Hunan Provincial Innovation Foundation for Postgraduate (CX2017B083). The authors appreciate the reviewers and the editor for their careful reading and many constructive comments and suggestions on improving the manuscript.

References

[1] Li L, Zhao D, Sun X. Nonorthogonality analysis of acoustics and vorticity modes: Should thermoacoustic energy norm be time-invariant? Aerosp Sci Technol 2018;77:149–55.
[2] Liu X, Deng B, Fu J, Xu Z, Liu J, Li M, et al. The effect of air/fuel composition on the HC emissions for a twin-spark motorcycle gasoline engine: a wide condition range study. Chem Eng J 2019;355:170–80.
[3] Chen X, Li J, Feng M, Zhao D, Shi B, Wang N. Flame stability and combustion characteristics of liquid fuel in a meso-scale burner with porous media. Fuel 2019;251:249–59.
[4] Zhang Z, Jiaqiang E, Chen J, Zhu H, Zhao X, Han D, et al. Effects of low-water addition on spray, combustion and emission characteristics of a medium speed diesel engine fueled with biodiesel fuel. Fuel 2019;239:245–62.
[5] Shu J, Fu J, Liu J, Wang S, Yin Y, Deng B, et al. Influences of excess air coefficient on combustion and emission performance of diesel pilot ignition natural gas engine by coupling computational fluid dynamics with reduced chemical kinetic model. Energ Convers Manage 2019;187:283–96.
[6] Mansour C, Bounif A, Aris A, Gaillard F. Gas-Diesel (dual-fuel) modeling in diesel engine. Int J Therm Sci 2001;40:409–24.
[7] Imran S, Emberson DR, Diez A, Wen DS, Crookes RJ, Korakianitis T. Natural gas fueled compression ignition engine performance and emissions maps with diesel and RME pilot fuels. Appl Energ 2014;124:354–65.
[8] Namasivayam AM, Korakianitis T, Crookes RJ, Bob-Manuel KDH, Olsen J. Biodiesel, emulsified biodiesel and dimethyl ether as pilot fuels for natural gas fuelled engines. Appl Energ 2010;87:769–78.
[9] Fu J, Shu J, Zhou F, Liu J, Xu Z, Zeng D. Experimental investigation on the effects of compression ratio on in-cylinder combustion process and performance improvement of liquefied methane engine. Appl Therm Eng 2017;113:1208–18.
[10] Meng X, Tian H, Long W, Zhou Y, Bi M, Tian J, et al. Experimental study of using additive in the pilot fuel on the performance and emission trade-offs in the diesel/CNG (methane emulated) dual-fuel combustion mode. Appl Therm Eng 2019;157:113718.
[11] Zheng J, Wang J, Zhao Z, Wang D, Huang Z. Effect of equivalence ratio on combustion and emissions of a dual-fuel natural gas engine ignited with diesel. Appl Therm Eng 2019;146:738–51.
[12] Chen Z, Wang L, Yuan X, Duan Q, Yang B, Zeng K. Experimental investigation on performance and combustion characteristics of spark-ignition dual-fuel engine fueled with methanol/natural gas. Appl Therm Eng 2019;150:164–74.
[13] Yang B, Ning L, Chen W, Wang B, Zeng K, Dong W. Parametric investigation the particle number and mass distributions characteristics in a diesel/natural gas dual-fuel engine. Appl Therm Eng 2017;127:402–8.

[14] Castro N, Toledo M, Amador G. An experimental investigation of the performance and emissions of a hydrogen-diesel dual fuel compression ignition internal combustion engine. Appl Therm Eng 2019;156:660–7.
[15] Liu J, Zhao H, Wang J, Zhang N. Optimization of the injection parameters of a diesel/natural gas dual fuel engine with multi-objective evolutionary algorithms. Appl Therm Eng 2019;150:70–9.
[16] Zhang Z, Zhao D, Ni S, et al. Experimental characterizing combustion emissions and thermodynamic properties of a thermoacoustic swirl combustor. Appl Energy 2019;235:463–72.
[17] Jung J, Song S, Hur KB. Numerical study on the effects of intake valve timing on performance of a natural gas-diesel dual-fuel engine and multi-objective Pareto optimization. Appl Therm Eng 2017;121:604–16.
[18] Cameretti MC, Tuccilo R, De Simio L, Iannaccone S, Ciaravola U. A numerical and experimental study of dual fuel diesel engine for different injection timings. Appl Therm Eng 2016;101:630–8.
[19] Abagnale C, Cameretti MC, De Simio L, Gambino Iannaccone S, Tuccilo R. Numerical simulation and experimental test of dual fuel operated diesel engines. Appl Therm Eng 2014;65:403–17.
[20] Zhou H, Li X, Lee C. Investigation on soot emissions from diesel-CNG dual-fuel. Int J Hydrogen Energ 2019;44:9438–49.
[21] Shu J, Fu J, Liu J, Ma Y, Wang S, Deng B, et al. Effects of injector spray angle on combustion and emissions characteristics of a natural gas (NG)-diesel dual fuel engine based on CFD coupled with reduced chemical kinetic model. Appl Energy 2019;233–234:182–95.
[22] Shu J, Fu J, Liu J, Zhang L, Zhao Z. Experimental and computational study on the effects of injection timing on thermodynamics, combustion and emission characteristics of a natural gas (NG)-diesel dual fuel engine at low speed and low load. Energ Convers Manage 2018;160:426–38.
[23] Li L, Wang JX, Wang Z, Liu HY. Combustion and emissions of compression ignition in a direct injection diesel engine fueled with pentanol. Energy 2015;80:575–81.
[24] Rahimi A, Fatehifar E, Saray R, Khoshbakhti. Development of an optimized chemical kinetic mechanism for homogeneous charge compression ignition combustion of a fuel blend of n-heptane and natural gas using a genetic algorithm. Proc IMechE Part D 2010;224(9):1141–59.
[25] Zhang J, Hu E, Zhang Z, Pan L, Huang Z. Comparative study on ignition delay times of C1–C4 alkanes. Energ Fuel 2013;27(6):3480–7.
[26] Zhao D, Gutmark E, Goey P. A review of cavity-based trapped vortex, ultra-compact, high-g, inter-turbine combustors. Prog Energ Combust 2018;66:42–82.
[27] Wang CHJ, Zhao D, Schlüter J, Holzäpfel F, Stephan A. LES study on the shape effect of ground obstacles on wake vortex dissipation. Aerosp Sci Technol 2017;63:245–58.
[28] Han Z, Reitz RD. Turbulence modeling of internal combustion engines using RNG k-e models. Combust Sci Technol 1995;106:267–95.
[29] Richards K, Senecal P, Pomraning E. CONVERGE (version 2.3.19) manual. Madison, WI: Convergent Science Inc; 2016.
[30] Amsden AA, O' Rourke PJ, Butler TD. KIVA-II: a computer program for chemically reactive flows with sprays (Technical Report LA-11560-MS). Los Alamos National Laboratory; 1989.
[31] Post SL, Abraham J. Modeling the outcome of drop–drop collisions in Diesel sprays. Int J Multiphas Flow 2002;28:997–1019.
[32] Schmidt DP, Rutland CJ. A new droplet collision algorithm. J Comput Phys 2000;164:62–80.
[33] Beale JC, Reitz RD. Modeling spray atomization with the Kelvin-Helmholtz/Rayleigh-Taylor hybrid model. Atom Spray 1999;9:623–50.
[34] Gonzalez DM, Lian ZW, Reitz R. Modeling diesel engine spray vaporization and combustion. SAE Trans 1992;101:1064–76.
[35] Heywood JB. Internal combustion engine fundamentals. 2nd ed. New York: McGraw-Hill; 2018.
[36] Jiang X, Zhang Y, Man X, Pan L, Huang Z. Shock tube measurements and kinetic study on ignition delay times of lean DME/n-butane blends at elevated pressures. Energ Fuel 2013;27(10):6238–46.
[37] Jiang X, Deng F, Yang F, Huang Z. Ignition delay characteristic and kinetic investigation of DME/n-pentane binary mixture: Interpreting the effect of equivalence ratio and DME blending. Energ Fuel 2018;32:3814–23.
[38] Jiang X, Deng F, Yang F, Zhang Y, Huang Z. High temperature ignition delay time of DME/n-pentane mixture under fuel lean condition. Fuel 2017;191:77–86.
[39] Jiang X, Zhang Y, Man X, Pan L, Huang Z. Experimental and modeling study on ignition delay times of DME/n-butane blends at pressure of 2.0 MPa. Energ. Fuel 2014;28(3):2189–98.
[40] Curran HJ, Gaffuri P, Pitz WJ, Westbrook CK. A comprehensive modeling of n-heptane oxidation. Combust Flame 1998;114:149–77.
[41] Zhang J, Niu S, Zhang Y, Tang C, Jiang X, Hu E, et al. Experimental and modeling study of the auto-ignition of n-heptane/n-butanol mixtures. Combust Flame 2013;160(1):31–9.
[42] Zhang Y, Huang Z, Wei L, Zhang J, Law C. Experimental and modeling study on ignition delays of lean mixtures of methane hydrogen oxygen argon at elevated pressures. Combust Flame 2012;159(3):918–31.
[43] Zhang Y, Jiang X, Wei L, Zhang J, Tang C, Huang Z. Experimental and modeling study on auto-ignition characteristics of methane/hydrogen blends under engine relevant pressure. Int J Hydrogen Energ 2012;37(24):19168–76.
[44] Aggarwal SK, Awomolo O, Akber K. Ignition characteristics of heptane–hydrogen and heptane–methane fuel blends at elevated pressures. Int J Hydrogen Energ 2011;36:15392–402.
[45] Yousefi A, Birouk M. Investigation of natural gas energy fraction and injection timing on the performance and emissions of a dual-fuel engine with pre-combustion chamber under low engine load. Appl Energ 2017;189:492–505.
[46] Turns SR. An introduction to combustion concepts and applications. 3rd ed. New York: McGraw-Hill; 2012.
[47] Hill SC, Douglas Smoot L. Modeling of nitrogen oxides formation and destruction in combustion systems. Prog Energ Combust 2000;26:417–58.
[48] Metcalfe WK, Burke SM, Ahmed SS, Curran HJ. A hierarchical and comparative kinetic modeling study of C1–C2 hydrocarbon and oxygenated fuels. Int J Chem Kinet 2013;45:638–75.
[49] Liu J, Yang F, Wang H, Ouyang M, Hao S. Effects of pilot fuel quantity on the emissions characteristics of a CNG/diesel dual fuel engine with optimized pilot injection timing. Appl Energ 2013;110:201–6.